DOI https: //doi. org/10.1007/s11595-019-2116-9

Influence of Si Content on Properties of $Ti_{(1-x)}Si_xN$ Coatings

WAN Qiang[1], LIU Nian[1], YANG Bing[2], LIU Huidong[2], CHEN Yanming[2]

(1.School of Engineering, Huazhong Agricultural University, Wuhan 430070, China;
2.School of Power & Mechanical Engineering, Wuhan University, Wuhan 430072, China)

Abstract: To investigate the evolution of microstructure and wear behavior of TiSiN coatings with the variation of Si in targets and lays the foundation for its controllable mass production, $Ti_{(1-x)}Si_xN$ composite coatings were deposited onto Si (100) and cemented carbide substrates using TiSi targets with different Si content by cathodic arc ion plating. The influences of Si on the microstructure and mechanical properties were studied. Nano-amorphous composite structure appeared in the $Ti_{(1-x)}Si_xN$ coatings when Si content in TiSi target was higher than 5at%. However, further increase of Si content in TiSi target exhibited a negligible effect on the microstructure of $Ti_{(1-x)}Si_xN$ coatings. Hardness and deformation resistance were correlated to the content of Si in TiSi targets. Maximum hardness was obtained as the Si content in target increased up to 20at%. Friction coefficient and wear rate significantly decreased with addition of Si in TiN coating, and then dually increased with the increase of Si content in targets.

Key words: cathodic arc ion plating; $Ti_{(1-x)}Si_xN$ coating; silicon content; nanocomposite; mechanical properties; wear resistance

1 Introduction

$Ti_{(1-x)}Si_xN$, as a typical nano-composite coating, has been widely studied to explore applications in solar selective absorbing, biomedical implant[1-2]. The most promising application of $Ti_{(1-x)}Si_xN$ coating should be used as a good candidate for cutting tools due to its enhanced hardness, outstanding oxidation resistance and lower friction coefficient[3-5]. According to the published references, it has been successfully fabricated by using plasma-enhanced CVD[6], ion beam assisted deposition[7], reactive magnetron sputtering[8] and cathodic arc ion plating (CAIP)[9]. Among these technologies, CAIP is the suitable method for mass production of $Ti_{(1-x)}Si_xN$ coating due to its excellent adhesive force, and high deposition rate[10]. Using CAIP fabrication, Si could be introduced into TiN coating from TiSi alloy target or Si-containing gas sources. However, it has been reported that the Si-containing gas sources would induced high internal stress in $Ti_{(1-x)}Si_xN$ coatings[11]. Therefore, TiSi alloy target is considered as the most suitable silicon source for $Ti_{(1-x)}Si_xN$ coating for the batch production in industrial scale[11]. As reported, the microstructure, mechanical properties, and cutting performance can be significantly influenced by deposition conditions such as target current, bias voltage, especially the Si content in target[12-14]. The bias voltage in industrial production is an important deposition parameter, which exhibits great influence on the crystallization orientation and the internal stress of the coatings[15]. Silicon content also plays a critical role on the microstructure and properties of $Ti_{(1-x)}Si_xN$ coating[16]. According to the thermodynamic phase diagram, Ti-Si-N coatings will form a solid solution structure when the Si content is lower than 3at% and transform into a nanocomposite structure when the Si content falls in the range of 3at% to 12at%[17]. The effects of Si on the microstructure, mechanical properties, and wear resistance of $Ti_{(1-x)}Si_xN$ coating have been researched intensively[18,19]. However, most of published works use the mixed gases of Ar_2 and N_2 in the chamber as the working ambient, which is different from the industrial batch production where the pure nitrogen gas is used to make sure the high batch repetition and stability. Therefore, it is an interesting investigation on the effect of Si content in TiSi target on the mirostructure and mechanical properties of the coating with high bias voltage at pure N_2 for the industrial production of $Ti_{(1-x)}Si_xN$ composite coating.

(Received: May 11, 2018; Accepted: July 22, 2018)

WAN Qiang(万强): Ph D; E-mail: wanqiang0915@163.com

Funded by the National Natural Science Foundation of China (U1832127)

This paper mainly focuses on the effects of Si content of TiSi target on the microstructure and compositions of $Ti_{(1-x)}Si_xN$ coating by cathodic ion plating. Then, the nanohardness and tribological behavior are investigated systemically. The results are expected to be helpful for the understanding of strengthen mechanism of $Ti_{(1-x)}Si_xN$ coating and exploring the industrials batch production of $Ti_{(1-x)}Si_xN$ coating.

2 Experimental

2.1 Specimens preparation

Ti-Si-N coatings were deposited on mirror polished Si (100) substrates (for structural analysis) and cemented carbide substrates (for mechanical measurements) by cathodic arc ion plating system using Ti, $Ti_{95}Si_5$, $Ti_{90}Si_{10}$, $Ti_{85}Si_{15}$, and $Ti_{80}Si_{20}$ alloy targets. The TiSi alloy targets were synthesized by hot press technology at 10^{-2} Pa with well mixed 400 mush Ti and Si powders. The size of the chamber was 540 mm × 295 mm × 395 mm, the minimum distance between samples and source was 225 mm. Prior to deposition, Ar^+ ion bombardment was carried out to remove the contamination on the substrate surface in Ar atmosphere at 2×10^{-2} Pa, then a TiN interlayer and $Ti_{(1-x)}Si_xN$ composite coatings were deposited with a rotation speed of 4rpm. TiN interlayer was employed to increase the adhesion strength between the substrate and $Ti_{(1-x)}Si_xN$ coating. More details of deposition parameters were listed in Table 1.

Table 1 Deposition conditions

Parameters	Value
Target size	φ100
Target materials/at%	Ti, $Ti_{95}Si_5$, $Ti_{90}Si_{10}$ $Ti_{85}Si_{15}$, $Ti_{80}Si_{20}$
Substrate bias voltage/V	Bombarding: −800; deposition: −150
Working gas	N_2
Base pressure/Pa	7.0×10^{-3}
Working pressure, N/Pa	2.0
Arc current/A^2	60
Substrate temperature/℃	280
Rotation speed/rpm	4
Deposition time/min	30

2.2 Coating characterization

Surface morphologies of the as-deposited $Ti_{(1-x)}Si_xN$ coatings were observed by an FEI Sirion IMP SEM system. Semi-quantitative compositional analysis of the coatings was carried out using energy dispersive spectrometer analysis. X-ray diffraction (Bruker-axs D8 with a Cu K_α radiation –$\lambda_{K\alpha}$=0.15418 nm) was used to obtain the phase structure of the as-deposited samples. The grain size of TiN was calculated from XRD pattern by Debye-Scherrer equation. After ultrasonic cleaning in acetone and deionnized water, the binding energy of Si was detected by X-ray photoelectron spectroscopy (XPS Thermo Scientific Escalab 250 Xi spectrometer.). Cross-sectional analysis verification was done by HR-TEM (JEOL JEM 2010)

The tribological behaviors were evaluated on the MS-T3000 ball-on-disk tester under the room temperature and atmospheric pressure. Zirconia balls with a diameter of 3mm were chosen as mated materials. The reciprocating sliding test was carried out with a load of 5 N, the sliding speed was 200 rpm and the total testing time was 30 min. After wear tests, the morphologies of each wear scar were observed by laser confocal scanning microscopy (LCSM OLS4100). Furthermore, the chemical compositions of the micro-zone inside the scars had been characterized by energy dispersive X-ray spectroscopy with an abbreviation less than 10%. In addition, the nanohardness of the coatings was measured by nano-indentation (G200, Agilent technologies, USA).

3 Results and discussion

3.1 Microstructure of coatings

Fig.1 shows the surface morphologies and cross-sections of $Ti_{(1-x)}Si_xN$ coatings deposited with $Ti_{95}Si_5$ and $Ti_{80}Si_{20}$ targets. Particles and pin holes have been observed in the surface which is typical feature of cathodic arc ion plating[20]. These particles are resulted from solidification of the droplets, while holes are resulted from the peeling of particles. From the cross-sectional images, the thickness of $Ti_{(1-x)}Si_xN$ coatings deposited by $Ti_{95}Si_5$ is thicker than the thickness of $Ti_{(1-x)}Si_xN$ coatings deposited by $Ti_{80}Si_{20}$. TiN interlayer is observed which agrees well with the deposition process. As shown in Table 2, the Si content in the coatings increases from 2.9at% to 7.6at% when the Si in target increases from 5at% to 20at%. The Si content in coatings increased with the increase of Si in alloy targets. It should be noted that the ration of Si/Ti in coatings were all lower than that of the targets. The phenomenon should be attributed to the composition demixing effect which derives from the difference ionizing states of Ti and Si. Ti ions with a higher mean valence state of 2.05 reveal a better converging to the substrate compared with Si ions which present a mean valence state of 1.46 under high bias voltage. Thus, more Ti ions could be obtained in the substrate. In addition, Si ions could be

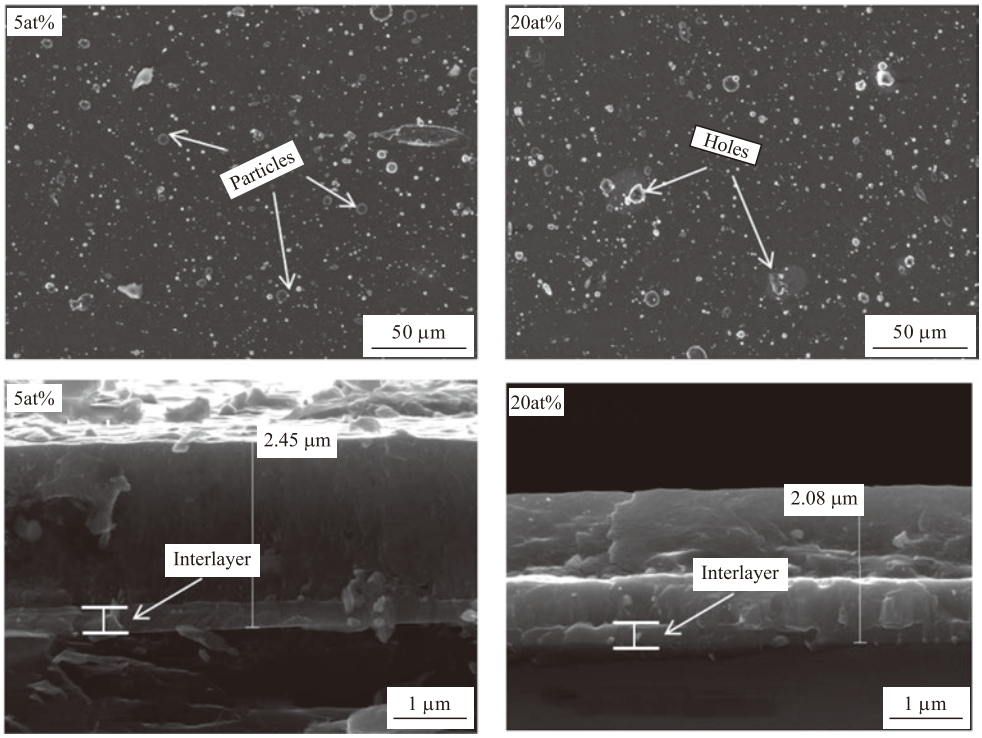

Fig.1 Surface morphology and cross-sections of coatings with different silicon contents

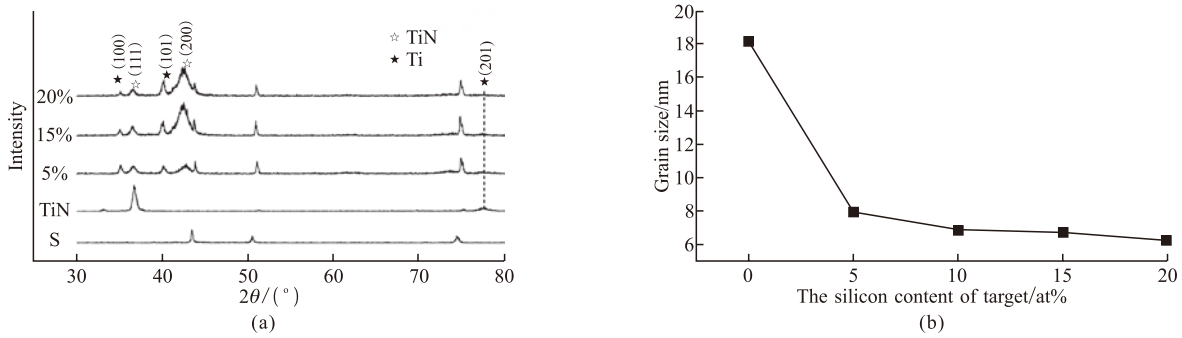

Fig.2 XRD study of coatings deposited with different silicon contents: (a) XRD patterns; (b) grain size evolution

easily bunched off from the substrate because of its higher velocity which is obtained from the electrical field between the target and substrate. As a result, the further incorporation of Si into the $Ti_{(1-x)}Si_xN$ composite coating would be hindered[21].

Table 2 Compositions of TiN and Ti-Si-N coatings

	Ti/at%	Si/at%	N/at%
Ti	56.1		43.9
$Ti_{95}Si_5$	47.1	2.9	50.0
$Ti_{90}Si_{10}$	46.0	5.2	48.8
$Ti_{85}Si_{15}$	45.8	6.6	47.6
$Ti_{80}Si_{20}$	36.8	7.6	55.6

As shown in Fig.2(a), the diffraction patterns consisted of cubic TiN, and hexagonal close-packed (hcp) Ti peaks as well as three substrate diffraction peaks. Three Ti peaks are resulted from these particles in the surface as shown in Fig.1. The preferred orientation of TiN coating and the $Ti_{(1-x)}Si_xN$ coating deposited with $Ti_{95}Si_5$ target is TiN (111) at 36.7° and transforms to TiN (200) as Si content in target increases up to 10at%. The preferred orientation change is related to the competition between surface energy and strain energy[22]. It should be noted that $Ti_{(1-x)}Si_xN$ coating deposited with pure Ti target in silane atmosphere reveals TiN (111) preferred orientation, which is different from the current (111) and (200) orientations of $Ti_{(1-x)}Si_xN$ coating in this work[15,21].

Fig.2(b) shows the grain size of all coatings in function of the Si content in targets. The grain size is calculated from the preferred orientation according to the Debye-Scherrer formula. TiN coating reveals a grain size of 18 nm while the grain sizes of $Ti_{(1-x)}Si_xN$ coatings are under 8 nm. In addition, the grain size of $Ti_{(1-x)}Si_xN$ coatings slightly decrease to 6 nm as silicon in targets increase to 20%. For all $Ti_{(1-x)}Si_xN$ coatings,

no evidence of crystalline SiN_x is detected. To investigate the state of Si, XPS spectra of Ti-Si-N coatings are shown in Fig.3.The banding energy of Si 2p is 102.1 eV which is in agreement with Si_3N_4. XRD and XPS results prove that Si exists in amorphous Si_3N_4 form in $Ti_{(1-x)}Si_xN$ coatings regardless of the silicon content in target.

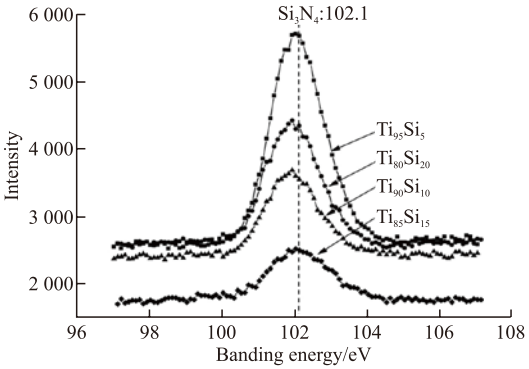

Fig.3 XPS spectra of Si 2p in Ti-Si-N coatings

Fig.4 shows the cross-sectional bright field (BF)-TEM images of TiN, $Ti_{(1-x)}Si_xN$ deposited with $Ti_{90}Si_{10}$ and $Ti_{85}Si_{15}$ on Si substrate. With the increase of Si content, the microstructure of coatings transforms from columnar grain to nanocrystalline composite in the coatings. The calculated lattice space for $Ti_{(1-x)}Si_xN$ coating deposited by $Ti_{90}Si_{10}$ is 3.49 Å, which is very close to the standard value for Ti_2N (110). The reason that Ti_2N phase has not been observed by XRD should be attributed to the small amount in coatings. For $Ti_{(1-x)}Si_xN$ coating deposited with pure Ti and $Ti_{85}Si_{15}$ targets, the lattice parameters *a* are 4.19 and 4.10 Å which correspond to that of TiN (a_0=4.2417 Å). The calculated lattice parameter of TiN is smaller than the standard value. The reason should be related to the formation of substituted solid solution (Ti, Si_x)N in which smaller Si atoms are introduced into TiN lattice to replace larger Ti atoms. Similar phenomenon also has been observed in other Me-Si-N coatings[17,23]. A careful study of the XRD patterns reveals a shift of TiN diffraction peaks towards higher angels which also identifies the lattice parameter change. The mean grain size of TiN coating observed from TEM is 18.9 nm, while the grain size of $Ti_{(1-x)}Si_xN$ coating deposited with $Ti_{90}Si_{10}$ and $Ti_{85}Si_{15}$ targets were 7.9 nm and 5.6 nm. The results agree well with the results calculated from XRD pattern. As Si in target increased from 10at% to 20at%, the compositions and grain size remain nearly stable.

3.2 Nano-indentation

TContinuous stiffness measurement (CSM) is used to measure nanohardness and elastic modulus of the coatings on tungsten carbide substrates. The measured hardness and elastic modulus against 800 nm indentation depth with Poisson's ratio 0.25 of multilayer films on tungsten carbide substrates are presented in Table 3. The data of hardness and elastic modulus presented are calculated using rule of thumb of 7%-15% of film thickness to minimize the substrate artifact and the effect of surface roughness. The measured nanohardness and elastic modulus of TiN coating are 27.4 GPa and 486 GPa, which are comparable with other studies[11]. $Ti_{(1-x)}Si_xN$ coatings deposited with $Ti_{90}Si_{10}$, $Ti_{85}Si_{15}$, $Ti_{80}Si_{20}$ possess higher hardness and lower elastic modulus compared with TiN coating. It suggests that the incorporated Si greatly enhances mechanical properties of TiN coating[13,24]. The nanohardness of $Ti_{(1-x)}Si_xN$ coatings increase with the increase of Si in

Table 3 Mechanical properties of TiN and Ti-Si-N coatings

Target	Ti	$Ti_{95}Si_5$	$Ti_{90}Si_{10}$	$Ti_{85}Si_{15}$	$Ti_{80}Si_{20}$
Hardness/GPa	27.4±0.6	27.5±1.3	25.1±1.1	30.4±1.5	34.2±1.6
Young's modulus, *E**/GPa	486.6±22	397±18	374±14	500±23	473±21
H^3/E^{*2}/GPa	0.09	0.13	0.113	0.11	0.18

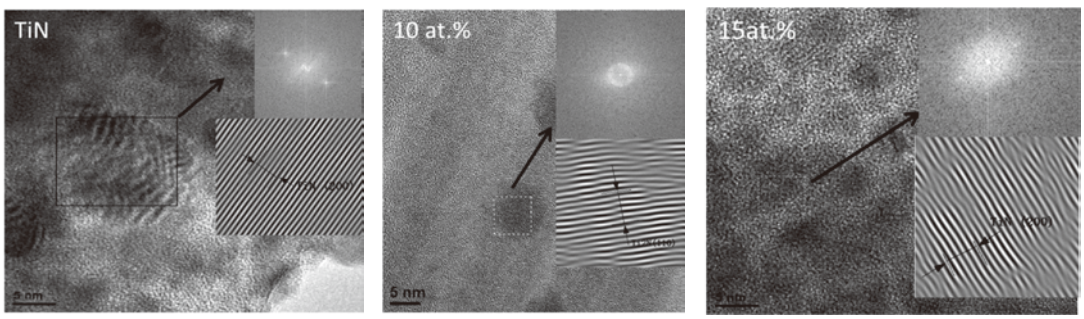

Fig.4 TEM micrographs of coatings deposited with different silicon content

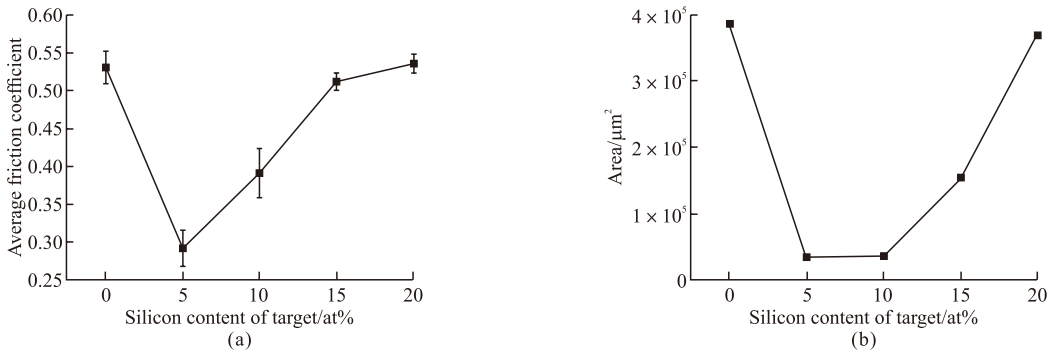

Fig.5 Friction coefficient and wear rate coatings deposited with different silicon contents

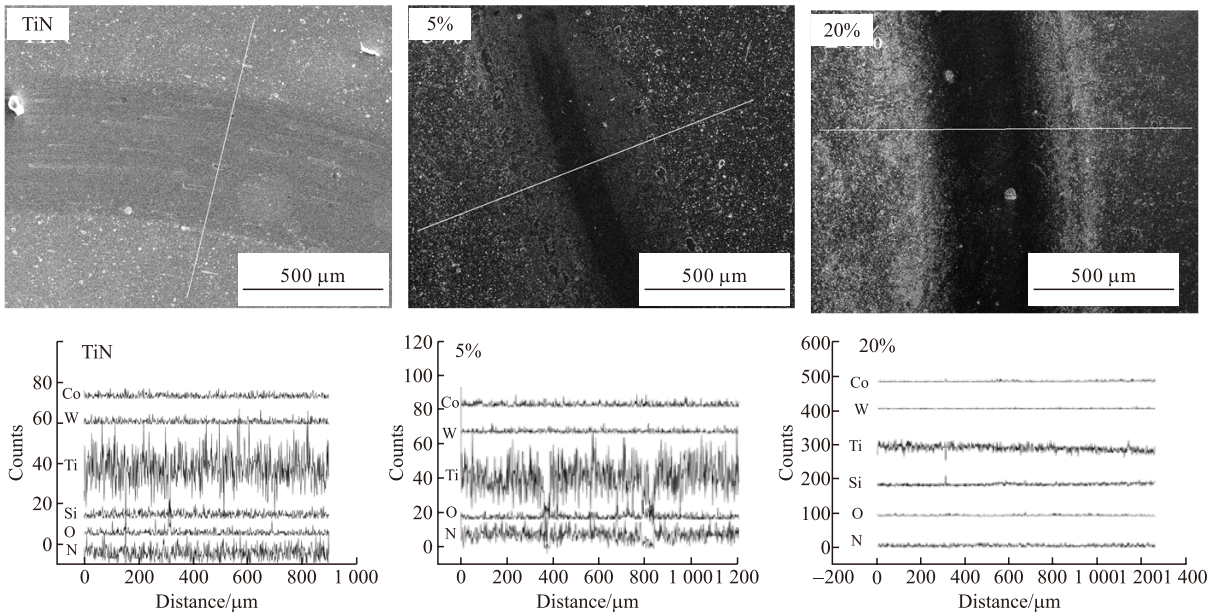

Fig.6 SEM images of the wear scar and EDX line analysis

targets. The maximum hardness with a value of 34.2 GPa is obtained in coatings deposited by $Ti_{80}Si_{20}$ target.

In order to enhance the resistance to plastic deformation, it is necessary to obtain materials that possess high hardness but lower elastic modulus value[25]. This behavior could be expressed by the H^3/E^{*2} ratio, where H and E^* are the hardness and effective modulus of the coating, respectively. E^* is expressed as $E^* = E/(1-\nu^2)$, where E is the Young's modulus, and ν is the Poisson ratio (about 0.25)[26]. The value of H^3/E^{*2} against the Si content in targets are shown in Table 3. According to the results, the resistance of elastic deformation increase with increase of Si content in TiSi targets. The best resistance to plastic deformation is obtained in $Ti_{(1-x)}Si_xN$ coating deposited with $Ti_{80}Si_{20}$ target.

3.3 Friction behaviors

As shown in Fig.5, TiN coating reveals the highest friction coefficient with a value of 0.53, while $Ti_{(1-x)}Si_xN$ coatings have lower average friction coefficient and present better anti-wear properties than TiN coating. The reported average friction coefficient of TiSiN coating deposited with pure Ti target in silane range from 0.6 to 0.7[15], which are much higher than that in this work. To further investigate the wear resistance of these coatings, the wear rate ($m^3/m{\cdot}N$) is calculated from the profiles of wear scars of these coatings after reciprocating sliding test by the formula in the Ref.[27]. The calculated results show that the wear rates of $Ti_{(1-x)}Si_xN$ coatings are much lower than TiN coating. It indicate that $Ti_{(1-x)}Si_xN$ coatings presented better friction resistance than TiN coating. As Si content increased, wear rate of $Ti_{(1-x)}Si_xN$ coatings increase significantly. The similar change in the average friction coefficient and wear rate confirms that the increase of Si in target would greatly increase wear rate and friction coefficient.

According to the friction test results, Si reveals great effect on the friction coefficient and wear rate. To study detailed affect mechanism, morphologies of the wear scar are observed by SEM and EDS. In literatures,

the lower friction coefficient of $Ti_{(1-x)}Si_xN$ coating is attributed to the finer grain or the lubrication of Si because of the formation of hydrate reactions SiO_2 or $Si(OH)_2$[27]. To check the tribology mechanisms, SEM morphologies of wear scar and the EDS line scan analysis have been carried out (as shown in Fig.6). No variation of O is observed across the wear scars of $Ti_{(1-x)}Si_xN$ coatings deposited with $Ti_{0.95}Si_{0.05}$ and $Ti_{0.8}Si_{0.2}$ targets which means that the reported hydrate reaction $Si_3N_4+6H_2O\rightarrow 3SiO_2+4NH_3$ does not reacted. Thus, the reported hydrate reactions come from the counterpart ball and water in air rather than the $Ti_{(1-x)}Si_xN$ coatings[29]. Therefore, the lower friction coefficient of $Ti_{(1-x)}Si_xN$ coatings is derived from the fine grain.

3.4 Discussion

According to the literature, the cutting performance of tools is largely dependent on the hardness and friction behavior of cutting tools[30]. This is the reason why so many works have been achieved to develop coatings with super hardness and low friction coefficient. In this paper, the average friction coefficient and wear rate of $Ti_{(1-x)}Si_xN$ coatings are lower than TiN coating, which confirms that the $Ti_{(1-x)}Si_xN$ coatings present better wear resistance. The excellent wear resistance of $Ti_{(1-x)}Si_xN$ is resulted from its higher hardness. It is worth noting that the hardness and plastic deformation resistance of $Ti_{(1-x)}Si_xN$ coatings increase with Si content in target, though the friction coefficient and wear rate also increase. The results suggest that wear resistance of coatings not only depend on hardness. As shown in Fig.6, the wear scar of TiN coating is much broader than that of $Ti_{(1-x)}Si_xN$ coatings which is consistence well with results of wear rate. Coating deposited with $Ti_{0.95}Si_{0.05}$ has the lowest friction coefficient and wear rate. However, obvious exfoliation (sliding ploughed grooves) and accumulation of debris can be observed around wear scars. This indicates the wear mechanism is a combination of adhesion and abrasion. For $Ti_{(1-x)}Si_xN$ coatings deposited with TiSi, only debris layer has been observed. The accumulated debris around the wear scar should be the only phenomena of degradation for coating deposited with high Si content. It can be concluded that $Ti_{(1-x)}Si_xN$ coatings deposited with $Ti_{95}Si_5$ target reveals a combination of adhesion and abrasion wear mechanism due to its low hardness, while $Ti_{(1-x)}Si_xN$ coatings deposited with Si higher than 5at% only presents an abrasion wear mechanism. The increase of friction coefficient and wear rate of $Ti_{(1-x)}Si_xN$ coatings should be related to the high roughness of coatings. As the Si content increases, the melting point of target decreases and lead to the increase of particle density (as shown in Fig.1). The increase of particle density indicates a higher roughness which would lead to an increase of friction coefficient and wear rate, especially in abrasion wear mechanism. Similar phenomenon also has been observed in the Refs.[31,32]. Thus, the work to reduce the particle density in TiSiN coatings with high hardness should be further studied to meet the industrial application in cutting tool.

4 Conclusions

$Ti_{(1-x)}Si_xN$ composite coatings are deposited by cathode arc ion plating system on polished Si(100) and cemented carbide. Effects of Si content on the microstructure and friction behaviors are investigated. Following conclusions can be obtained:

a) $Ti_{(1-x)}Si_xN$ coatings deposited with more than 5at% Si in target consists of TiN nanocrystalline and amorphous Si_3N_4 phase. Si content in coatings firstly increase as that in target increase, and reaches the maximum content 6.5at% at $Ti_{90}Si_{10}$ target. The increase of Si in target leads to a grain refinement from 18.9 nm to 5.6 nm.

b) The hardness and plastic deformation of $Ti_{(1-x)}Si_xN$ coatings increase with the increase of Si in TiSi targets. The highest hardness and best plastic deformation resistance obtained in $Ti_{(1-x)}Si_xN$ coating deposited with $Ti_{80}Si_{20}$ target are 34.2 and 0.18 GPa, respectively.

c) $Ti_{(1-x)}Si_xN$ coatings possesses lower friction coefficient and wear rate in comparison with TiN coating. As the Si in target increase, the friction coefficients and wear rates of $Ti_{(1-x)}Si_xN$ coatings increase and the wear mechanism transforms from a combination of adhesion and abrasion to only abrasion.

References

[1] Zhang M, Ma S, Xu K, *et al.* Vascular Endothelial Cell Compatibility of Superhard Ternary Ti-Si-N Coatings with Different Si Contents[J]. *Vacuum,* 2014, 106(ASM6): 53-63

[2] Feng J, Zhang S, Liu X, *et al.* Solar Selective Absorbing Coatings TiN/TiSiN/SiN Prepared on Stainless Steel Substrates[J]. *Vacuum,* 2015, *121:* 135-141

[3] Ishikawa T, Obata F, Inoue K. Wear Mechanism of TiSiN -Coated Cutting Tools on High-Speed Cutting of Hardened Die Steel[J].*Journal of the Japan Society for Precision Engineering,* 2009, *75*(12): 1 439-1 443

[4] Bouzakis KD, Skordaris G, Gerardis S, *et al.* Ambient and Elevated Temperature Properties of TiN, TiAlN and TiSiN PVD Films and Their Impact on the Cutting Performance of Coated Carbide Tools[J]. *Sur-*

face & Coatings Technology, 2009, 204(6-7): 1 061-1 065

[5] Caliskan H , Celil CC , Panjan P. Effect of Multilayer Nanocomposite TiAlSiN/TiSiN/TiAlN Coating on Wear Behavior of Carbide Tools in the Milling of Hardened AISI D2 Steel[J]. *Journal of Nano Research,* 2016, 38: 9-17

[6] Jedrzejowski P, Klemberg-Sapieha JE, Martinu L. Quaternary Hard Nanocomposite TiCxNy /SiCN Coatings Prepared by Plasma Enhanced Chemical Vapor Deposition[J]. *Thin Solid Films,* 2004, 466(1-2): 189-196

[7] Zhang C, Luo J, Li W, *et al.* Mechanical Properties of Nanocomposite TiN/Si_3N_4 Films Synthesized by Ion Beam Assisted Deposition (IBAD) [J]. *Journal of Tribology,* 2003,125(2): 445

[8] Kim SH, Kim JK, Kim KH. Influence of Deposition Conditions on the Microstructure and Mechanical Properties of Ti-Si-N Films by DC Reactive Magnetron Sputtering[J]. *Thin Solid Films,* 2002, 420-421: 360-365

[9] Wan Q, Yang B, Liu HD, *et al.* Ion Irradiation Tolerance of Ti-Si-N Nanocomposite Coating[J]. *Surface & Coatings Technology,* 2016, 305*:* 165-169

[10] Chang CL, Lin CT, Tsai PC, Ho, *et al*. Y. Influence of Bias Voltages on the Structure and Wear Properties of Ti-Si-N Coating Synthesized by Cathodic Arc Plasma Evaporation[J]. *Thin Solid Films,* 2008, 516(16): 5324-5329.

[11] Li S, Deng J, Yan G, *et al.* Effects of Nitrogen Flowrates on Properties of TiSiN Coatings Deposited by Arc Ion Plating Combining with Medium-Frequency Magnetron Sputtering[J]. *International Journal of Refractory Metals & Hard Materials,* 2014, 42(1): 108-115

[12] Li S, Deng J, Qin X, *et al.* Effects of Ti Target Current on Properties of TiSiN Coatings[J]. *Surface Engineering*, 2016: 1-7

[13] Chang CL, Lin CT, Tsai PC, *et al.* Influence of Bias Voltages on the Structure and Wear Properties of TiSiN Coating Synthesized by Cathodic Arc Plasma Evaporation[J]. *Thin Solid Films,* 2008, 516(16): 5 324-5 329

[14] Dang C, Li J, Wang Y, *et al.* Influence of Multi-Interfacial Structure on Mechanical and Tribological Properties of TiSiN /Ag Multilayer Coatings[J]. *Journal of Materials Science*, 2016*,* 52(5): 1-13

[15] Yang Z, Zhu L, Yang B, *et al.* Structure and Properties of Ti-Si-N Coatings Synthesized by Combining Cathode Arc and Middle-Frequency Magnetron Sputtering[J]. *Journal of Wuhan University of Technology-Mater. Sci. Ed.,* 2009, 24(5): 702-705

[16] Tian CX, Yang B, Wan Q, *et al.* Effects of Sih_4 Flow Rate on Microstructure and Mechanical Properties of Tisin Nanocomposite Coatings by Cathodic Arc Ion Plating[J]. *Vacuum*, 2015, 117: 12-16

[17] Zhang CH, Lu XC, Wang, *et al.* Microstructure, Mechanical Properties, and Oxidation Resistance of Nanocomposite Ti-Si-N Coatings[J]. Applied Surface Science, 2006, 252(18): 6 141-6 153

[18] Flink A, Larsson T, Sjölén J, *et al.* Influence of Si on the Microstructure of Arc Evaporated (Ti,Si)N Thin Films; Evidence for Cubic Solid Solutions and Their Thermal Stability[J]. *Surface & Coatings Technology,* 2005, 200(5-6): 1 535-1 542

[19] Cheng YH, Browne T, Heckerman B, *et al.* Influence of Si Content on the Structure and Internal Stress of the Nanocomposite Tisin Coatings Deposited by Large Area Filtered Arc Deposition[J]. *Journal of Physics D Applied Physics,* 2009, 42(12): 125 415

[20] Sanchette F, Ducros C, Schmitt T, *et al.* Nanostructured Hard Coatings Deposited by Cathodic Arc Deposition: From Concepts to Applications[J]. *Surface & Coatings Technology,* 2011, *205*(23) :5 444-5 453

[21] Chang CL, Lin CT, Tsai PC, *et al.* Influence of Bias Voltages on the Structure and Wear Properties of TiSiN Coating Synthesized by Cathodic Arc Plasma Evaporation[J]. *Thin Solid Films,* 2008, 516(16) : 5 324-5 329

[22] Zou CW, Wang HJ, Li M, *et al.* Characterization and Properties of Tin-Containing Amorphous Ti–Si–N Nanocomposite Coatings Prepared by arc Assisted Middle Frequency Magnetron Sputtering[J]. *Vacuum,* 2010, 84(6): 817-822

[23] Bendavid A, Martin PJ, Cairney J, *et al*. Deposition of Nanocomposite Tin /Si_3N_4, Thin Films by Hybrid Cathodic arc and Chemical Vapor Process[J]. *Applied Physics A,* 2005, 81(1): 151-158.

[24] Yang SM, Chang YY, Lin DY, *et al.* Mechanical and Tribological Properties of Multilayered TiSiN /CrN Coatings Synthesized by a Cathodic Arc Deposition Process[J]. *Surface & Coatings Technology,* 2008, 202(10): 2 176-2 181

[25] Benkahoul M, Robin P, Gujrathi SC, *et al.* Microstructure and Mechanical Properties of Cr-Si-N Coatings Prepared by Pulsed Reactive Dual Magnetron Sputtering[J]. *Surface & Coatings Technology,* 2008, 202(16): 3 975-3 980

[26] Song M, Sun Y, He Y. Structure Dependent Hardness and Elastic Modulus of FeCuSiBAl Amorphous/Nanocrystalline Alloys[J]. *Materials Science & Engineering A,* 2012, 556: 974-976

[27] Musil J, Kunc F, Zeman H, *et al.* Relationships Between Hardness, Young's Modulus and Elastic Recovery in Hard Nanocomposite Coatings[J]. *Surface & Coatings Technology,* 2002, 154(2-3): 304-313

[28] Bousser E, Benkahoul M, Robin P, *et al.* Effect of Microstructure on the Erosion Resistance of Cr-Si-N Coatings[J]. *International Conference on Metallurgical Coatings and Thin Films-ICMCTF*. 2008

[29] E Török, AJ Perry, L Chollet, *et al.* Young's Modulus of TiN, TiC, ZrN and HfN[J]. *Thin Solid Films,* 1987, 153(1-3): 37-43

[30] SP Li, JX Deng, GD Zhang, *et al.* Dry Cutting Performance of Tools Deposited with TiSiN-WS_2/Ti-WS_2 Coatings[J]. *Surface Engineering,* 2015, 31:12 949-12 956

[31] Mo JL, Zhu MH, Lei B, *et al.* Comparison of Tribological Behaviours of AlCrN and TiAlN Coatings-Deposited by Physical Vapor Deposition[J]. *Wear,* 2007, 263(7): 1 423-1 429

[32] Cheng YH, Browne T, Heckerman B, *et al*. Mechanical and Tribological Properties of Nanocomposite Tisin Coatings[J]. *Surface & Coatings Technology,* 2010, 204(14): 2 123-2 129